EPJ Web of Conferences **40**, 15014 (2013)
DOI: 10.1051/epjconf/20134015014

Growth, structure, surface topography and magnetic properties of $GdMnO_3$ multiferroic epitaxial thin films

N. Andreev[1], V. Chichkov[1], T. Sviridova[1], N. Tabachkova[1], A. Volodin[2], C. Van Haesendonck[2], and Ya. Mukovskii[1]

[1]National Science and Technology University "MISiS", Leninskii prosp., 4, Moscow, 119049, Russia
[2]Laboratory of Solid State Physics and Magnetism, KU Leuven, Celestijnenlaan 200 D, BE-3001, Leuven, Belgium

Abstract. Epitaxial $GdMnO_3$ thin films were grown in various regimes on (001) $NdGaO_3$ and (001) $SrTiO_3$ substrates by RF magnetron sputtering. X-ray analysis revealed that the films grown at a substrate temperature of 650-900 °C are single phase ($GdMnO_3$ with orthorhombic *Pbnm* structure). Films grown on $NdGaO_3$ substrates at lower temperature (< 750 °C) have only one out-of-plane orientation, i.e. $GdMnO_3(001)||NdGaO_3(001)$, whereas films grown at higher temperatures (> 750 °C) reveal two orientations, i.e. $GdMnO_3(001)||NdGaO_3(001)$ and $GdMnO_3(110)||NdGaO_3(001)$. These results are confirmed by transmission electron microscopy. Films grown on $SrTiO_3$ substrates have two orientations, i.e. $GdMnO_3(001)||SrTiO_3(001)$ and $GdMnO_3(110)||SrTiO_3(001)$, in the whole temperature range in which the phase exists. Using atomic force microscopy the correlation between the topography of the films and their crystallographic structure was studied. The magnetic properties of the films differ from those of bulk samples and revealed spin-glass behavior.

1 Introduction

Multiferroic materials, which simultaneously exhibit electric polarization and magnetic ordering, are the subject of significant research interest due to the intriguing physical mechanism and potential applications for tunable multifunctional devices [1-4]. In particular, multiferroic manganites $RMnO_3$ (R = Gd-Lu, Y, Sc) have attracted considerable attention [2,4-8]. It has been found that the electric polarization can be caused by the non-polar lattice distortion in hexagonal manganites(R = Ho-Lu, Y, Sc) or by the cycloidal antiferromagnetic structure in the orthorhombic manganites (R = Gd-Dy) [2,4]. The fact that the magnetic ordering induces the ferroelectric state is the reason for the high magnetic tunability of the electrical properties of the orthorhombic manganites [2].

Among the orthorhombic multiferroic manganites, $GdMnO_3$ has a special place because it is located on the magnetic phase diagram for $RMnO_3$ compounds very close to the phase boundary between A-type anti-ferromagnetic and cycloidal antiferromagnetic phases [5-7]. As a consequence the ferroelectric and the magnetic properties of this compound are quite complicated [6]. Bulk $GdMnO_3$ has an orthorhombic structure (o-GMO, space group *Pbnm*) with lattice parameters a = 5.310 Å, b = 5.840 Å and c = 7.430 Å [8] at room temperature. It undergoes an antiferromagnetic transition at $T_N \approx 42$ K when the Mn^{3+} magnetic moments are ordering into the incommensurate sinusoidal antiferromagnetic structure [5,6]. On further cooling, at $T_{lock} \approx 23$ K, the magnetic structure changes to a canted A-type antiferromagnetic structure [6,7]. Below T ≈ 6.5 K a long-range ordering of the Gd^{3+} magnetic moments occurs [6,7]. The application of a magnetic field exceeding 1 T along the *b*-axis at temperatures below T ≈ 13 K turns the o-GMO into a ferroelectric state. This effect has been related to ordering of the Gd^{3+} magnetic moments, probably stabilizing a cycloidal antiferromagnetic ordering of the Mn^{3+} magnetic moments [6].

Intensive research efforts have recently been devoted to the o-GMO epitaxial thin films [9-11]. It is well known that the epitaxial thin film materials may exhibit unique physical properties which can be very different from those of the bulk because of strain related stress (due to the film-substrate lattice misfit) and due to the contribution of the surface. Hence it has become important to investigate the influence of the substrate and of the film growth conditions on the thin film properties. Here, we describe the synthesis, crystal structure, surface morphology and magnetic properties of o-GMO thin films prepared by magnetron sputtering.

2 Experimental

The o-GMO thin films were deposited by RF-magnetron sputtering with the "facing-target" scheme [12,13]. This

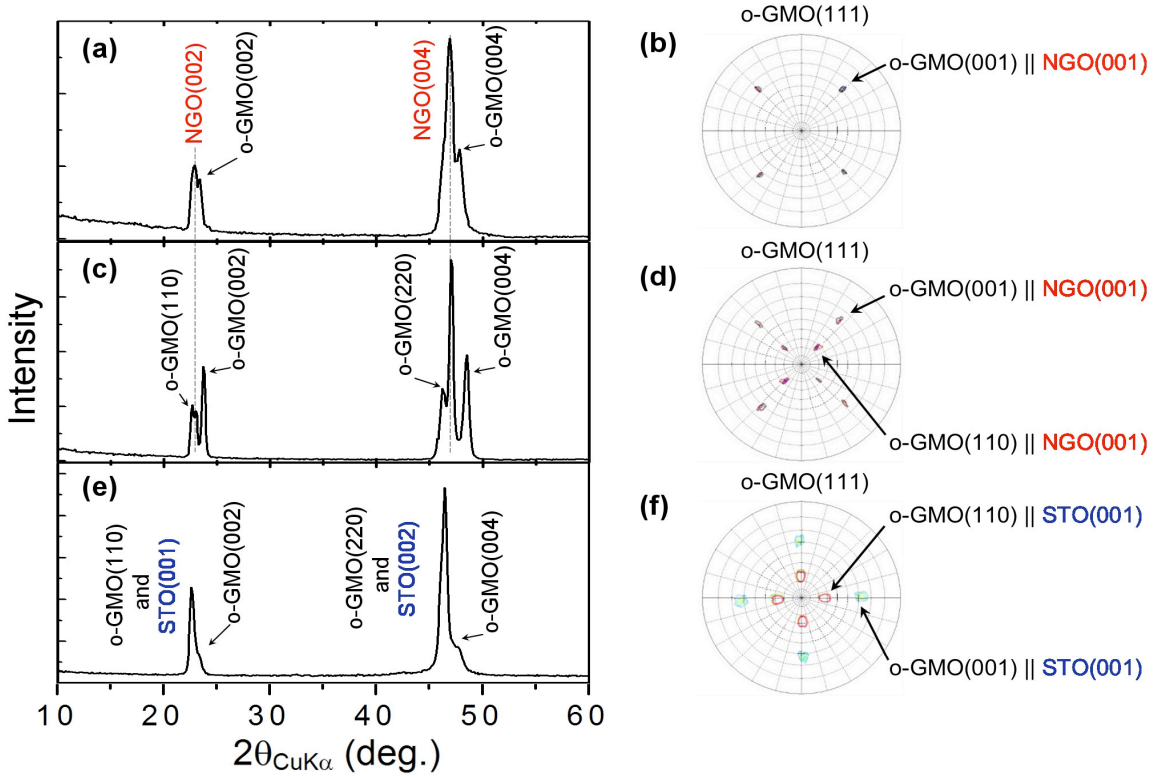

Fig. 1. *θ–2θ* XRD patterns and pole figures of the (111) reflections of o-GMO films grown on a NGO(001) substrate at a temperature (a,b) below 750 °C and (c,d) above 750 °C, and (e,f) grown on a STO(001) substrate.

scheme allows to transfer elements from a target to a substrate without changes in the composition. Therefore sputtering could be carried out from stoichiometric single phased targets prepared by solid-state synthesis using Gd_2O_3 and MnO_2 oxides powders. The films were grown on orthorhombic (001)-oriented $NdGaO_3$ (NGO) (space group *Pbnm; a* = 5.431 Å, *b* = 5.499 Å, *c* = 7.710 Å [14]) and cubic (001)-oriented $SrTiO_3$ (STO) (*a* = 3.90 Å) substrates The deposition temperature ranged between 650 °C and 900 °C and the films were grown in an atmosphere consisting of a mixture of Ar and O_2 with pressure 1-2 mTorr. The thickness of the o-GMO films was 100-130 nm. The structure of the thin films was determined by X-ray diffraction (Rigaku Ultima, using CuK_α radiation), electron diffraction and high resolution transmission electron microscopy (Jeol JEM-2100). The surface topography of the films was analyzed by atomic force microscopy (Dimension 3100 from Bruker). The magnetic properties of the o-GMO films were measured using a commercial SQUID magnetometer (Quantum Design MPMS-5XL).

3 Results and discussion

X-ray analysis indicated that in all cases single phase o-GMO films were grown. On the other hand, the texture of the films depended on the type of substrate and the deposition temperature. Figure 1a presents a *θ–2θ* XRD pattern typical for the o-GMO||NGO samples grown at a temperature below 750 °C. Visible peaks correspond to multiple reflections from the (001) planes of the NGO substrate and the o-GMO film. This suggests that the films are textured, with the out-of-plane orientation o-GMO(001)||NGO(001). The out-of-plane $d_{(001)}$ the *c* lattice parameter of o-GMO is 7.6 Å, i.e. somewhat increased with respect to the value for bulk material (c_{bulk} = 7.43 Å). The strain is $\varepsilon_{(001)}$ = 2.3%. The pole figure of the (111) o-GMO reflections of this sample is presented in figure 1b. Four o-GMO(111) peaks can be observed at the ϕ-positions 48°/132°/228°/312° and ψ = 62 . The corresponding ϕ–positions of the NGO substrate (111) reflections are 45.5/134.5/225.5°/314.5° (not presented). This allows us to conclude that the o-GMO grows in such a way that the film in-plane parameters *a* and *b* are placed on the rectangular NGO lattice (a_{NGO} = 5.431 Å × b_{NGO} = 5.499 Å) with the following epitaxial relationship: [100]GMO(001)||[100]NGO(001).

For the samples grown at a substrate temperature above 750 °C we observe two additional reflections from the (110) plane of the o-GMO phase in the *θ–2θ* scan (figure 1c) and a group of four additional peaks at ψ = 28 in the pole figure (figure 1d). This is consistent with the coexistence of two types of domains with different out-of-plane orientation: o-GMO(001)||NGO(001) and o-GMO(110)||NGO(001). When the (110) film plane is parallel to the (001) NGO substrate plane, the rectangular lattice of the film with sides c_{GMO} = 7.430 Å × $\sqrt{a_{GMO}^{\ 2} + b_{GMO}^{\ 2}}$ = 7.806 Å is placed within the diagonal spacing of the *ab*-plane of the NGO substrate ($\sqrt{a_{NGO}^{\ 2} + b_{NGO}^{\ 2}}$ = 7.72 Å), with corresponding epitaxial relationship [001]GMO(110)||[110]NGO(001). As the result of the formation of a second orientation, the out-of-plane lattice parameter for the first orientation

$d_{(001)}$ = 7.51 Å decreases and approaches to the bulk value. The strain is $\varepsilon_{(001)}$ = 1.1%.

The films on $SrTiO_3$ substrates have two types of out-of-plane orientations for the whole temperature range in which the phase exists. The θ–2θ scan and the pole figure of the (111) o-GMO reflections for the o-GMO film deposited on a STO (001) substrate are presented in figure 1e and figure 1f, respectively. Reflections from the (001) and (110) planes of the o-GMO are present in the θ–2θ scan. The (110) o-GMO reflections coincide with the (001) STO reflections. The presence of two groups of peaks at $\psi = 28$ and $\psi = 62$ in the pole figure confirms that the film has two different out-of-plane orientations, i.e. o-GMO(001)||STO(001) (peaks at ψ = 62) and o-GMO(110)||STO(001) (peaks at $\psi = 28$). The first group of peaks at $\psi = 62$ can be considered as four 90° shifted sets of pairs of peaks separated by 4.6° A similar situation was observed for the case of orthorhombic $YMnO_3$(001)||STO(001) films [15]. The splitting of the o-GMO(111) peaks results from the presence of 90° in-plane twinning. The small mismatch between the film and the substrate lattice results from the fact that the lattice of the film is rotated by 45 relative to the substrate (001) plane, implying GMO is growing on the $a_{STO}\sqrt{2}$ = $3.9\sqrt{2}$ Å × $a_{STO}\sqrt{2}$ = $3.9\sqrt{2}$ Å square STO lattice. The two in-plane 90°-rotated domains are formed due to the fourfold symmetry in the plane of the substrate with epitaxial relationships [100]GMO(001)||[110]STO(001) and [010]GMO(001)||[110]STO(001).

For the second orientation o-GMO(110)||STO(001) the rectangular lattice of the film is placed within the spacings 2*a* and 2*b* of the STO(001). The epitaxial relationships are [001]GMO(110)||[100]STO(001) and [001]GMO(110)||[010]STO(001).

The X-ray results for the films on the NGO substrate were confirmed by transmission electron microscopy (TEM). Figures 2a and 2b present the TEM images of a o-GMO||NGO sample grown at a temperature below 750°C. The o-GMO film presented in figures 2a and 2b has a thickness of about 140 nm and a columnar structure. Figure 2c presents a high-resolution transmission electron microscopy (HRTEM) image and the corresponding electron diffraction (ED) patterns that were obtained from a cross section along the [010] zone of the NGO substrate. The ED patterns provide clear evidence for the heteroepitaxial growth of the film on the substrate. The HRTEM image indicates that the interface between the substrate and the film is relatively flat and well-defined. The film has a good crystalline quality with distinct atomic arrangements.

The TEM images of a o-GMO||NGO sample grown at a temperature above 750 °C are presented in Figures 2d and 2e. The o-GMO film reveals the presence of domains having a second orientation with the *c*-axis lying in the substrate plane, i.e. different from the first main orientation with the *c*-axis perpendicular to the substrate.

The atomic force microscopy (AFM) images and line profiles of o-GMO films grown on NGO(001) (a) and STO(001) (b) substrates are presented in figure 3. The films display smooth surface with a root mean square

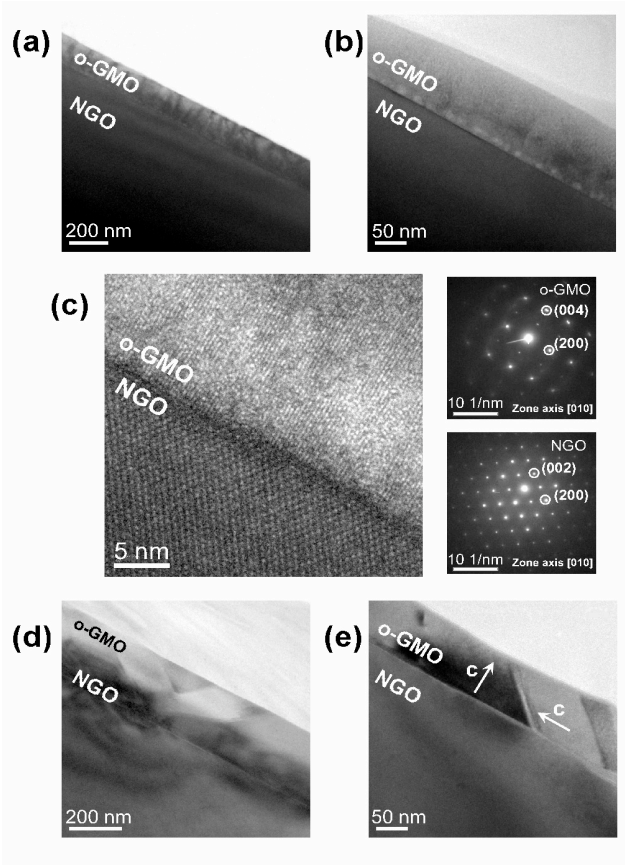

Fig. 2. TEM images of o-GMO films on a NGO(001) substrate grown at a temperature (a,b) below 750 °C and (d,e) above 750 °C; (c) HRTEM image revealing the interface regions of a o-GMO(001)film on a NGO(111) substrate and the ED patterns for the film and the substrate.

roughness ranging from 0.5 to 1 nm (for NGO) and from 1 to 1.5 nm (for STO) with small (50 to 100 nm) islands-like grains. The AFM image for a film on a NGO substrate clearly correlates with the TEM image (figure 2a), revealing columnar (3D) growth. For the films on a STO substrate one observes in the AFM images two differently oriented types of ellipse-like grains, which correspond to the in-plane 90°-rotated domains appearing in the XRD patterns..

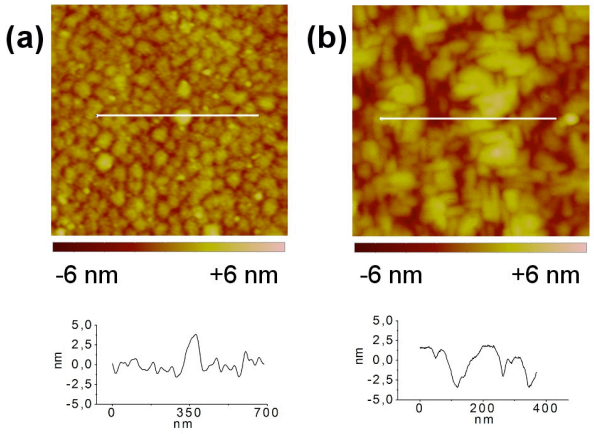

Fig. 3. AFM images and corresponding line profiles along the white lines for o-GMO films grown on (a) a NGO(001) substrate (1 μm^2 area) and (b) a STO(001) (0.25 μm^2 area) substrate

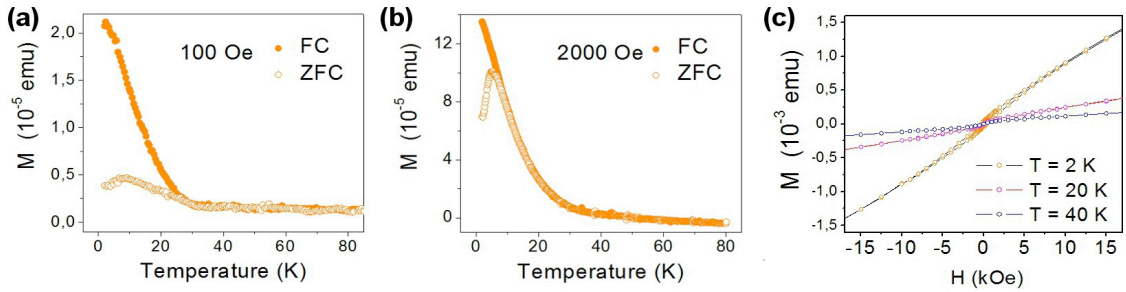

Fig. 4. Temperature dependence of the zero-field-cooled and field-cooled magnetization for a o-GMO film on a STO(001) substrate. Magnetic fields of (a) 0.1 kOe and (b) 2 kOe are applied perpendicular to the plane of the film. (c) Magnetic-field-dependence of magnetization at 2, 20, and 40 K.

For the magnetization measurements o-GMO films grown on STO substrates were used rather than films grown on NGO substrates. Measurements of the magnetization for o-GMO||NGO films are complicated by the large paramagnetic response of the NGO substrate. The NGO is paramagnetic with a large value of the Nd magnetic moment (3.5 $_B$/atom) and the paramagnetic response of the thick substrate masks the signal from the o-GMO film. Figure 4a gives the zero-field-cooled (ZFC) and the field-cooled (FC) magnetization as a function of temperature acquired for a o-GMO||STO sample in a magnetic field of 100 Oe applied perpendicular to the plane of the film. A dramatic difference in the temperature dependences of the magnetization under FC and ZFC conditions is clearly observed at temperatures below 35 K. The difference in the temperature dependence appears close to the magnetic ordering temperature T_N of the bulk material around 42 K. Furthermore, the ZFC curve has a cusp around 10 K. The applied magnetic field increasing (2000 Oe, figure 4b) shifts the onset for the different temperature dependence and the cusp towards lower temperatures. These observations are consistent with the presence of a spin-glass behavior which results from the competing ferromagnetic-antiferromagnetic interactions. Figure 4c presents magnetization loops measured at 2, 20, and 40 K and confirms the presence of ferromagnetic order. Similar behavior has been observed in orthorhombic $YMnO_3$ [16], $YbMnO_3$ [17] and $TbMnO_3$ [18] thin films. This suggests that the spin-glass behavior is a common mechanism in orthorhombic manganite thin films.

4 Acknowledgments

The authors thank N.N. Volkov (Kirensky Institute of Physics, SB RAS) for magnetic property measurements, the Materials Science and Metallurgy Joint Use Center (NUST “MISiS”) for the TEM studies and A.E. Pestun (NUST “MISiS”) for the sputtering target fabrication. The work has been financially supported by the Research Foundation – Flanders (FWO), the Flemish Concerted Action (GOA) program and the RFBR grant № 12-02-00717_a.

References

1. M. Fiebig, J. Phys. D **38**, R123 (2005)
2. T. Kimura, T. Goto, H. Shintani, K. Ishizaka, T. Arima, and Y. Tokura, Nature **426**, 55 (2003)
3. R. Ramesh and N.A. Spaldin, Nature Mater. **6**, 21 (2007)
4. S.-W. Cheong and M. Mostovoy, Nature Mater. **6**, 13 (2007)
5. T. Kimura, S. Ishihara, H. Shintani, T. Arima, K. T. Takahashi, K. Ishizaka, and Y. Tokura, Phys. Rev. B **68**, 060403 (R) (2003)
6. T. Kimura, G. Lawes, T. Goto, Y. Tokura, and A.P. Ramirez, Phys. Rev. B **71**, 224425 (2005)
7. J. Hemberger, S. Lobina, H.-A. Krug von Nidda, N. Tristan, V. Yu. Ivanov, A. A. Mukhin, A. M. Balbashov, and A. Loidl, Phys. Rev. B **70**, 024414 (2004)
8. T. Mori, N. Kamegashira, K. Aoki, T. Shishido, and T. Fukuda, Mater. Lett. **54**, 238 (2000)
9. M.W. Kim, S. J. Moon, J. H. Jung, J. Yu, S. Parashar, P. Murugavel, J. H. Lee, and T.W. Noh, Phys. Rev. Lett. **96,** 247205 (2006)
10. E. Vlakhov, B. Blagoev, E. Mateev, L. Neshkov, T. Nurgaliev, L. Lakov, K. Toncheva, Y. Marinov, K. Nenkov, I. Radulov, K. Piotrowski, W. Paszkowicz, A. Szewczyk, M. Baran, and R. Szymczak, J. Optoelectron. Adv. M. **9**,456 (2007)
11. N. Andreev, N. Abramov, V. Chichkov, A. Pestun, T. Sviridova and Ya. Mukovskii, Acta Phys. Pol. A, **117**, 210 (2010)
12. Y. Hoshi, M. Naoe, and S. Yamanaka, Electron. Comm. Jpn. Pt. I **65**, 106 (1982)
13. E.A. Antonova, V.L. Ruzinov, S.Yu. Stark, and V.I. Tchitchkov, Supercond. Phys. Chem. Techn. **4**, 1624 (1991)
14. A. Marezio, J.P. Remeika, and P.D. Dernierr, Inorg. Chem. **7,** 1337 (1968)
15. X. Marti, F. Sánchez, V. Skumryev, C. Ferrater, M. V. García-Cuenca, M. Varela, and J. Fontcuberta, Thin Solid Films **516**, 4899 (2008)
16. X. Marti, V. Skumryev, V. Laukhin, F. Sánchez, M. V. García- Cuenca, C. Ferrater, M. Varela, and J. Fontcuberta, J. Mater. Res. **22**, 2096 (2007)
17. D. Rubi, S. Venkatesan, B. J. Kooi, J. T. M. De Hosson, T. T. M. Palstra, and B. Noheda, Phys. Rev. B **78**, 020408 (R) (2008)
18. D. Rubi, C. de Graaf, C. J. M. Daumont, D. Mannix, R. Broer, and B. Noheda, Phys. Rev. B **79**, 014416 (2009)